



Effect of backward median current on stability, microstructure, and mechanical properties of SUS304 weldments fabricated by local dry underwater MIG welding

Wenxu Zhang¹ · Haipeng Liao¹ · Bin Zhang¹ · Qin Zhang¹ · Xiangmiao Wu¹ · Jiyu Tian¹ · Zhenmin Wang¹

Received: 20 March 2023 / Accepted: 1 July 2023 / Published online: 8 July 2023
© The Author(s), under exclusive licence to Springer-Verlag London Ltd., part of Springer Nature 2023

Abstract

Local dry underwater backward median pulse MIG welding (LDU-BMPMIG) was proposed in this study. The effects of different backward median currents on welding process stability, weld forming, microstructure, and mechanical properties of weldments were investigated comprehensively. The results reveal that the backward median current waveform effectively improved the welding stability. By calculating the approximate entropy of the voltage signal during welding, it is proved that the welding stability increases first and then decreases with the increase of the backward median current. The welding process stability was the most satisfied with the backward median current of 200 A. The quality of weld formation was consistent with welding stability. LDU-BMPMIG weldments exhibited fewer macroscopic defects and better overall morphology compared with LDU-PMIG weldment. The weldment microstructure was mainly composed of γ -austenite and δ -ferrite with different morphologies. The satisfied stability of the welding process contributed to improving the microstructure uniformity. The variation trend of tensile strength for LDU-BMPMIG weldments was approximately kept consistent with welding process stability. The weldment prepared by 200 A showed considerable mechanical properties with minimal fluctuation, which reached 97.58% of maximum average tensile strength, which meant the most excellent compared to the others. The experimental results can improve the stability of local dry underwater welding and provide a theoretical basis and technical support for the application of underwater welding.

Keywords Local dry underwater welding · Backward median pulse · SUS304 · Welding stability · Weld performance

1 Introduction

Due to its high corrosion resistance, structural stability, high strength, and good weldability, 304 stainless steel is widely used in offshore platforms, offshore pipelines, ship repair, nuclear power equipment maintenance, and other fields. The aforementioned structures have been subjected to wave impact, corrosion damage, and other factors for a long time, which are facing a huge and urgent need for underwater repair. Underwater welding technology is gradually applied

to the emergency repair of large underwater structures for its high cladding rate and simple equipment [1]. The underwater welding technology is mainly divided into three types: wet welding, dry welding, and local dry underwater welding. The underwater wet welding technology has been initially applied in welding engineering; the main problems faced by this method are that the direct contact between the workpiece and water leads to a severe quenching effect, arc instability, and weld porosity caused by gas injection and the loss of alloying elements leads to decreased mechanical properties [2, 3]. The main problems of underwater dry welding are high cost and poor applicability. The local dry underwater method reduces the welding cost compared with the two methods; it reduces the influence of water on the stability of the welding arc, hydrogen diffusion, and hardening structure as much as possible. However, the current local dry underwater welding process is still immature. Improving the stability of the local dry underwater welding process and weld quality has become a hot research issue.

✉ Jiyu Tian
tianjiyu@scut.edu.cn

✉ Zhenmin Wang
wangzhm@scut.edu.cn

¹ School of Mechanical & Automotive Engineering, South China University of Technology, Guangzhou 510641, People's Republic of China

Han et al. [4] designed the micro-drain cover, which can effectively isolate the contact between arc combustion and water to ensure the smooth progress of underwater welding. Fourteen groups of local dry underwater welding experiments using DC waveform were carried out. The experiment showed that a good-quality weldment can be obtained under proper welding parameters, but the weldment showed some spatter. There are three standard droplet transition modes in pulse inert-gas welding (PMIG): multi-pulse one-drop, one-pulse one-drop, and one-pulse multi-drop. The one-pulse one-drop droplet transition mode has a stable arc, small splash, and excellent weld formation and is considered the best droplet transition mode. However, due to the complex droplet transition process, it is difficult to make a quantitative analysis due to the influence of various factors. Wang et al. [5] studied the influence of different pulse frequencies on the droplet transition mode of local dry underwater welding under the pulse welding current waveform. The experiment proved that with the increase of pulse frequency, the droplet transition frequency decreased, and the droplet transition mode had an essential influence on the weld formation; a smooth, continuous weld without obvious defects could be obtained under the droplet transition. Liao et al. [6, 7] established a numerical model of droplet transfer for local dry underwater MIG welding to study the effects of gas pressure, wire feed, speed, and pulse peak current on the droplet transfer process. Research points out that increased gas pressure would hinder the droplet transfer process, and increased wire feed speed would improve the droplet transfer speed. With the increase of peak current, the droplet transfer mode changed from a spherical transfer (200 A) to a single pulse drop (280 A), a pulse of multiple droplets (360 A) finally. Guo et al. [8] studied the influence of pulse current waveform on droplet transition. The experiment proved that proper waveform parameters could achieve stable droplet transition and that the pulse current waveform would not change the mechanical properties of the weld. When the pulsed waveform is used for welding, the electromagnetic force will increase as the peak value of the welding current increases, which is conducive to drop shedding, and the penetration ability of welding is enhanced. Tabrizi et al. [9] compared the effect of DC and pulse current on AISI 316L stainless steel joints in gas tungsten welding and proved that pulse current refined grain and improved mechanical properties of AISI 316L stainless steel joints compared with DC.

The above studies show that the pulse welding current waveform can obtain a better droplet transition mode under appropriate parameters. However, the underwater welding environment is complex, and the droplet transition stability is primarily affected by welding parameters, underwater environmental pressure, periodic generation and rupture of bubbles, and other factors. Improving welding stability and quality is challenging by controlling the pressure of

the underwater environment and the periodic generation of bubbles. Therefore, some scholars proposed novel welding waveforms to enhance welding quality and stability.

Wu et al. [10] proposed a two-wire pulsed gas-shielded welding process using a median current waveform. A high-speed digital camera and a digital oscilloscope simultaneously recorded the metal transfer process and voltage and current waveforms of different median currents. The mathematical model of the droplet diameter was established. The experimental results showed that the median current significantly affects the metal transition; the ideal droplet mode (one-pulse one-drop) can be achieved within the suitable range of the median current. For experimental and numerical simulation, Xu et al. [11] used three groups of welding current waveforms with the same peak and base currents but different median currents in the current decline stage. The experiment showed that the waveforms with a median current of 140 A exhibited better tolerance to welding speed. Wu et al. [12] proposed a fast-frequency pulsed ultra-inert gas (FFP-TIG) welding technology, which effectively reduced the problem of metal grain coarsening caused by high heat input in traditional TIG welding and effectively improved weld quality.

Although the novel welding waveform can effectively improve the welding quality, researchers still need to quantitatively evaluate the stability of the welding process, which is necessary for complex underwater welding. At present, a large number of researchers have proposed quantitative evaluation methods for welding stability. Huang et al. [13] introduced multi-scale entropy into arc current signals with different welding process parameters to study the relationship between arc electric signals and welding stability. Experiments showed that the multi-scale entropy distribution was closely related to the type and stability of short-circuiting transfer in the welding process; the more stable the welding process, the smaller the amplitude of the multi-scale entropy curve. By studying the characteristics of the arc sound signal, Yao et al. [14] found that the random mutation of the arc due to unstable factors such as spatter and short circuit increased the complexity and randomness of the arc sound signal. Based on the quantification method of sample entropy, a composite quantitative evaluation index-arc sound sample entropy was proposed, which can avoid the influence of different parameters on the quantitative results and quantitatively reflect the stability of the arc welding process. To evaluate the stability of pulsed metal inert gas welding of aluminum alloy, Nie et al. [15] analyzed pulsed current signals under different stability conditions based on modern digital signal processing methods such as approximate entropy and probability density. The pulse current signals in different aluminum alloy metal inert gas welding processes were studied, and the approximate

entropy algorithm was used to evaluate the pulse current signals. The relationship between pulse metal inert gas welding of aluminum alloy and pulse signals was proved by qualitative analysis. The above research showed that the stability of welding process can be judged quantitatively by mathematical methods effectively. The application of median current waveform in underwater welding is rarely reported. It is urgent to solve the stability of underwater welding.

In this study, for the inferior stability of underwater welding, the backward median waveform was innovatively applied to the local dry underwater welding process. The current and voltage parameters in the welding process were collected to analyze the stability of the welding process. The influence mechanism of different backward median currents on the microstructure and mechanical properties of the weldments was studied. The research results are expected to solve the problem of local dry underwater welding process stability and provide a theoretical basis for the engineering application of the local dry underwater backward median pulse welding process.

2 Experimental procedure

The local dry underwater welding experiment platform comprises six degrees of freedom manipulator, self-developed welding power supply with constant current external characteristics, oscilloscope, wire feeding mechanism, micro-drainage cover, etc. The surfacing welding of austenitic stainless steel plate was carried out in the middle welding experiment. The weldments were placed in a transparent glass pool with water; the distance between the weldments and the water surface was 200 mm. According to the previous research results, the welding speed was set to 12.6 mm/s [16]. The protective gas and drainage gas were mixed with Ar (98%) and CO₂ (2%), and the pressure was 0.2 MPa. SUS 304 steel plate with a size of 300 mm × 100 mm × 5 mm was used as the base material in the experiment. ER 308LSi welding wire with a diameter of 1.2 mm was used as filler metal. The chemical compositions of the base metal and filler metal are shown in Table 1 (wt.%).

The backward median welding waveform adopted in this experiment is shown in Fig. 1. The backward median

Table 1 Chemical composition of base metal and filler metal

Material	C	Mn	S	Si	Cr	Ni	Mo	Fe
SUS304	0.059	1.00	0.003	0.53	18.18	8.10	0.03	Bal
ER 308Lsi	0.019	1.72	0.003	0.46	20.8	10.1	-	Bal

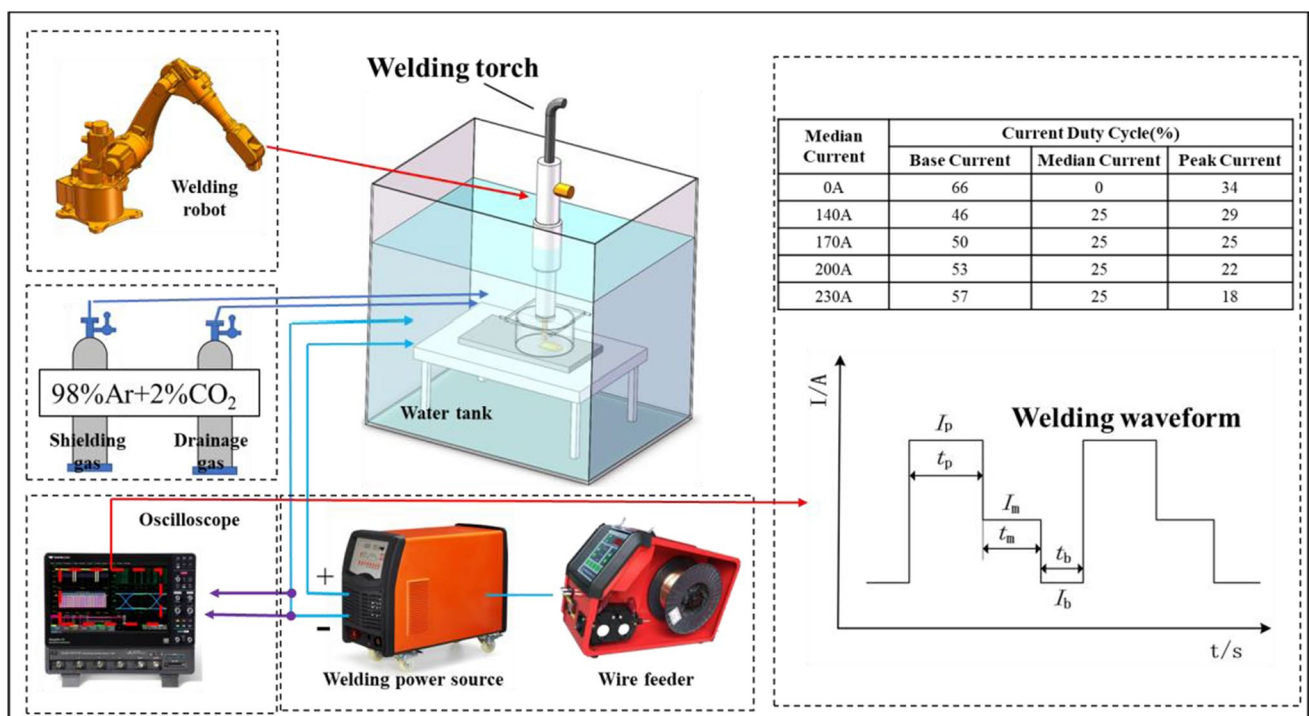


Fig. 1 Experimental platform and welding waveform

waveform is the insertion of a median current between the peak current and the base current. To explore the influence of different values of the backward median current on the stability of the welding process and the weldment's performance, it was necessary to set the welding current waveform reasonably before the formal experiment. When the pulse frequency ranges from 25 to 100 Hz, the electromagnetic force is the force that promotes the droplet transition, and the weld penetration can be effectively improved by increasing the welding frequency from 25 to 100 Hz. Therefore, the welding current waveform frequency was set as 100 Hz in this experiment [5, 17]. The magnitude of the current significantly affects the electromagnetic force, which can be determined by

$$F_{emz} = \frac{\mu_0 I^2}{4\pi} f_z \quad (1)$$

$$f_z = \left[\frac{1}{4} - \ln\left(\frac{r_d \sin\theta}{r_w}\right) + \frac{1}{1 - \cos\theta} - \frac{2}{(1 - \cos\theta)^2} \ln\left(\frac{2}{1 + \cos\theta}\right) \right] \quad (2)$$

where I is the welding current, r_d is the droplet radius, r_w is the electrode radius, θ is the angle of the arc root, and μ_0 is the vacuum permeability.

When the current increases, the electromagnetic force increases correspondingly and reaches the threshold value to promote the melting dripping, and the transition is completed [5]. When the traditional pulse current waveform is used for welding, the droplet grows at the base stage of the waveform and drops at the peak stage to complete the droplet transition. However, in the actual welding process, the arc in the underwater local dry environment is often interfered by water, air flow, etc., which leads to the droplet falling before it grows up or the droplet being too large before falling. Then, two droplet transitions occur in a particular welding cycle, or no droplet transitions occur in a specific welding cycle. Ultimately, the droplet transition is not uniform, the droplet size is inconsistent, and the welding voltage and current fluctuate abnormally, resulting in poor welding quality. Using the welding waveform containing the backward median current, selecting the appropriate backward median welding current size and the duty ratio of the backward median phase, on the one hand, the growth time of the droplet can be increased, making the droplet transition more stable and achieving the effect of one-pulse one-drop, improving the welding quality. On the other hand, it is equivalent in the peak stage and the base stage to avoid the wide range of welding current changes in the welding process, making the welding process more stable.

Five groups of experiments were designed. The base value of current waveform was set as 100 A to ensure normal arc combustion; the peak value of current waveform

was set as 300 A to ensure that the electromagnetic force reaches the threshold of droplet dripping [7]. To find a suitable median current value between the base current value and the peak current value, the median current cannot reach the threshold of droplet drop but also promote the growth of droplets. The backward median current of different groups was 0 A, 140 A, 170 A, 200 A, and 230 A; group 0 A used the pulse waveform. To ensure the effect reflected by the backward median current, the duty ratio of the backward median was kept at 25%. Too large or too small welding current would affect welding quality; hence, the average welding current of different groups was kept at 168 A. The average welding current can be calculated as follows:

$$I_{ave} = \frac{I_p t_p + I_m t_m + I_b t_b}{t_p + t_m + t_b} \quad (3)$$

where I_{ave} is the average current and I_p , I_m , and I_b are the peak current, backward median current, and base current of the waveform respectively. t_p is the peak current duration time, t_m is the backward median duration time, and t_b is the base current duration time. The duty ratio of peak current and base current can be calculated by Eq. 1, and the results are shown in Fig. 1.

Due to the large interference of air flow and water environment in the local dry underwater welding process, the welding process is relatively complicated. Multiple experiments were conducted on each group of welding parameters to eliminate the possible contingency of experimental results. The investigation was selected in which the welding effect of each group was relatively good without the phenomenon of arc breaking and wire sticking. The current and voltage signals are collected for welding stability analysis, and the three welds of each group were saved to analyze the mechanical properties of the weldments.

After welding, samples were cut from the weld with a wire cutter, and then polished and etched to obtain metallographic samples. The metallographic samples were etched with a mixture of hydrochloric acid and nitric acid (3:1), and the weld microstructure was observed with a Leica camera (DMI3000M). The tensile test used an electronic universal testing machine (DNS300), tensile speed of 2 mm/min, and the maximum load was 15 kN, refer to GB/T 228.1–2010. S-3700N observed the tensile fracture morphology.

3 Results and discussions

3.1 Stability analysis of welding process

In the welding process, the change of arc current and voltage signal waveform is closely related to the arc shape and

droplet transition type, and the phenomenon of arc breaking and short circuits in the welding process can be shown by the welding electrical signal [18]. Better arc shape and droplet transition type are essential to ensure the welding process stability. Collecting arc voltage and current parameters in the welding process is an effective method to analyze the stability of the welding process. Figure 2 is the voltage and current waveform collected during welding. High-voltage regions of voltage waveforms with different backward median values always appeared with the peak value of welding current. Due to the large duty ratio at the peak stage of current waveforms, the PMIG waveform (backward current was 0 A) displayed more high-voltage regions, and the voltage fluctuation range was also large. When the current jumped from the base value to the peak value, it was easy to appear a short-circuit point with zero voltage. The high-voltage region of the BPMIG waveforms was significantly less than that of PMIG waveform. The current waveform with the backward median value of 140 A and 170 A at the peak stage of current and the current waveform with the backward median value of 230 A at the backward median current stage both appeared unstable. The voltage and current waveform with the backward median value of 200 A showed small fluctuations and strong regularity, indicating good stability.

To more vividly analyze the stability of welding process, the trajectory of voltage and current parameters was drawn

as shown in Fig. 3. Figure 3b–e are the electrical signal collected in experiments with different backward median currents, and Fig. 3a is the electrical signal of PMIG waveform. The UI diagram shows the trajectory of voltage and current in the welding process, which can distinguish abnormal phenomena in the welding process, such as arc breaking and short circuits. In Fig. 3a, a certain number of short-circuit operating points with voltage less than or equal to zero appeared in zone I, and the voltage dropped rapidly during the short-circuit transition. Still, the current did not rise significantly due to the self-developed welding machine's active control of the welding current. In this short-circuit state, the distance between the welding wire and the molten pool was relatively close, and the temperature of the molten pool dropped rapidly during underwater welding; the extinguished arc led to wire sticking and reborn arc, resulting in poor weld continuity and spatter. In area II, the current decreased and the voltage increased, the arc length became unstable, and the arc extinguishing phenomenon occurred when the current was zero. Large voltage operating points appeared in area III, because the current should not change abruptly during welding, and the welding voltage will inevitably increase briefly when the current rapidly increases.

In Fig. 3, short circuits and arc breaking occurred less in normal welding conditions due to the appropriate welding speed and current selection. However, by comparing Fig. 3a to Fig. 3e, the BPMIG waveform displayed fewer

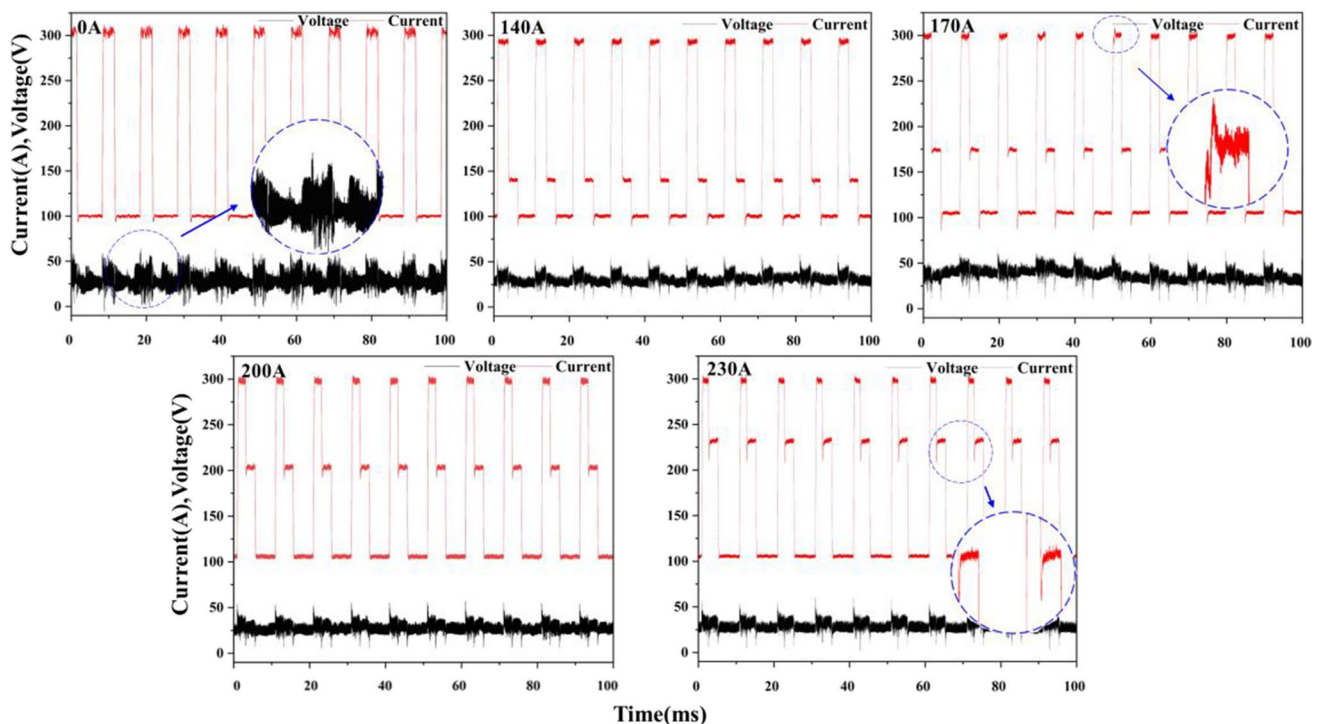


Fig. 2 Voltage and current waveforms

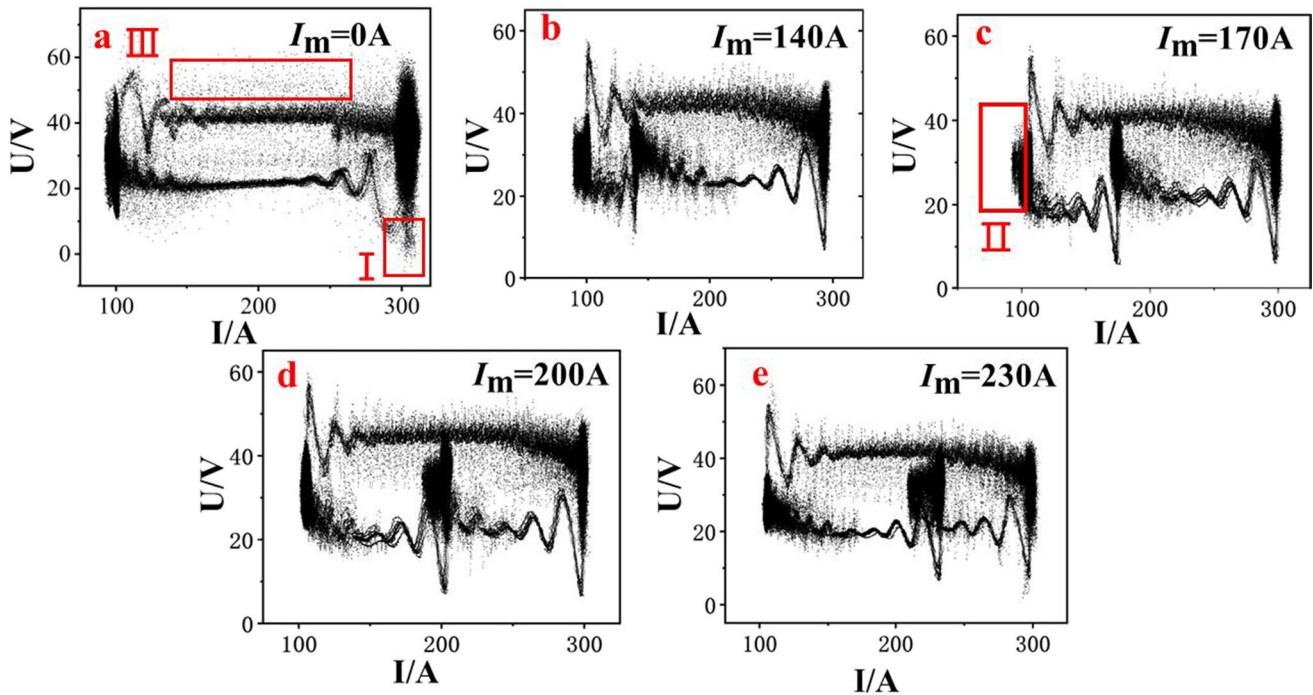


Fig. 3 Electrical parameter locus (a–e)

abnormal working tracks and a higher density of trace points than the PMIG waveform. Therefore, it can be concluded that the BPMIG waveform exhibited better stability than the PMIG waveform.

There are two main reasons for the improvement of welding stability. First, due to the median current between the peak current and the base current, the range of each change of welding current becomes smaller, which reduces the influence of the sudden change of current on the shape of the welding arc, and results in the periodic change of voltage stronger. In addition, the backward median current waveform changes the heat distribution, which can effectively control the droplet transition.

To further investigate and explore the influence of different backward median current waveforms on the stability, approximate entropy was used to evaluate the stability of the welding process. In 1990, Pincus [19] proposed the concept of approximate entropy to overcome the difficulty of solving entropy in chaotic phenomena. Approximate entropy is mainly used to measure the probability of generating new signal patterns. In the stable welding process, current and voltage changes should be periodic, so many scholars use approximate entropy to analyze the stability of the welding process quantitatively.

The approximate entropy algorithm is defined as follows: the one-dimensional time series $X(i)$ of data length N is reconstructed in m -dimensional phase space as follows:

$$X(i) = [x(i), x(i+1), \dots, x(i+m-1)] \quad (4)$$

where $i = 1, 2, 3, \dots, N-m+1$. The distance between space vectors $X(i)$ and $X(j)$ is defined as follows:

$$d[X(i), X(j)] = \max_{k=0,1,\dots,m-1} [|x(i+k) - x(j+k)|] \quad (5)$$

The correlation integral $C_i^m(r)$ can be defined as

$$C_i^m(r) = (N-m+1)^{-1} \times \sum_{j=1}^{N-m+1} \Theta\{r - d[X(i), X(j)]\} \quad (6)$$

where $\Theta(\cdot)$ is the Heaviside function, r is the allowable deviation, and $C_i^m(r)$ represents the probability that the distance between $X(i)$ and vector $X(j)$ is less than r , in other words, the degree to which $X(i)$ is related to all vector $X(j)$. The average autocorrelation degree $\{\Phi^m(r)\}$ of vector sequence $\Phi^m(r)$ can be defined as:

$$\Phi^m(r) = (N-m+1)^{-1} \sum_{i=1}^{N-m+1} \ln C_i^m(r) \quad (7)$$

The vector sequence $\Phi^m(r)$ decreases with the increase of m , indicating that the chance of state point association in the phase space of m dimension decreases with the increase of m . Approximate entropy is defined as:

$$S_a(m, r, N) = \Phi^m(r) - \Phi^{m+1}(r) \quad (8)$$

Pincus figured out that better results could be obtained if N was between 75 and 5000, $m = 1$ or $m = 2$, and $r = 0.1-0.2\sigma$ (σ is the standard deviation of the original data). In this paper, $m = 2$ and $r = 0.2\sigma$ were set.

To improve the speed of calculation, the collected current and voltage signals were reduced to 5000 in time sequence and equidistant. The average approximate entropy of current and voltage was calculated to draw the histogram as shown in Fig. 4. It was clear from Fig. 4 that the approximate entropy of the current was overall one order of magnitude smaller than that of voltage. The reason was that the self-developed constant current source welding power supply used in the experiment actively controls the current output, and the current output of the welding power supply displayed excellent periodicity, so the approximate entropy of the calculated current parameters was small. Compared with the current approximate entropy, the voltage parameter was more suitable to characterize the stability of the welding process. In Fig. 4, the approximate entropy of voltage decreased first and then increased when the backward median current gradually increased; the approximate entropy value and variance of approximate entropy were minimum at backward median current of 200 A. Figure 4 shows the voltage waveform segments collected from the welding process with the backward median value of 0 A, 140 A, and 200 A, among which the 200 A voltage waveform indicated better regularity, consistent with the calculated results.

This means welding with the backward median current of 200 A manifests better stability than welding with other backward median current waveforms. When the backward median current is 140 A or 230 A, the difference between the backward median current and the base or peak current is small, and the effect of the backward median current on the welding process is insignificant. On the contrary, because of frequent current adjustments, the stability of welding is

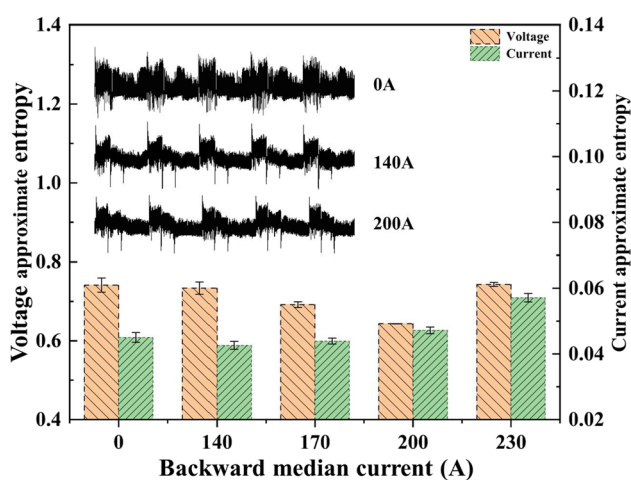


Fig. 4 Approximate entropy of current and voltage

reduced and affects welding quality. The backward median current of 200 A is below the threshold current that brings the droplet down; thus, the droplet falls in the peak phase of the current waveform after sufficient growth. In this case, the droplet transition is more regular and the stability of the welding process is improved.

3.2 Weld formation characteristics

3.2.1 Macroscopic morphological characteristics of weld

Figure 5 shows the weld morphologies prepared by different backward median current waveforms. The average length of the weldments was about 100 mm. The weldment's formation was good at suitable welding speed and electrical parameter; no obvious surface porosity, cracks, and other defects are seen, indicating that no serious short-circuit arc breaking phenomenon occurs in the welding process. Visible spatter was shown in the red box as shown in Fig. 5.

LDU-PMIG weldment exhibited poor formation with edge biting, spatter phenomenon, and poor uniformity. The forming effect of the LDU-BMPMIG weldment was significantly improved. Edge-biting defects can be seen in weldments prepared by backward median currents of 140 A and 230 A, as shown in the green box in Fig. 5. The temperature gradient during cooling and solidification of the welding pool is an important factor affecting the degree of weldment edge biting. The degree of biting of the weldment is mainly influenced by the temperature gradient of the weld pool; the arc breaking phenomenon may be caused by water intrusion in the welding process to affect the droplet transition process and heat input, which finally leads to an increased probability of weld edge biting. The weldments prepared by the median current of 170 A and 200 A showed fewer edge defects, smooth edge, and good uniformity, as shown in the black box in Fig. 5. The edge of the weldments was relatively flat, and the welding quality was good, indicating good welding stability was beneficial to reduce weldment defects.

Figure 6 shows the data of weld penetration, weld width, and weld reinforcement under different parameters. In Fig. 6, the weld penetration of the welds prepared with different backward median currents was all more than 2 mm, and the LDU-PMIG weld penetration value was obviously less than LDU-BMPMIG weld penetration. With the increase of the backward median current, the weld penetration first increased and then decreased, and reached the maximum value when the backward median value was 200 A. The main factor affecting the weld penetration value is the heat input. The average welding current and welding speed remained unchanged in the experiment; the weld penetration was difficult to show a large change [20]. However, due to the addition of backward median current in the welding process, the droplet grew completely, increasing the droplet impact

Fig. 5 Macroscopic morphology of weld and weld section

Median current	Weld appearance	Cross section morphology
0A		
140A		
170A		
200A		
230A		

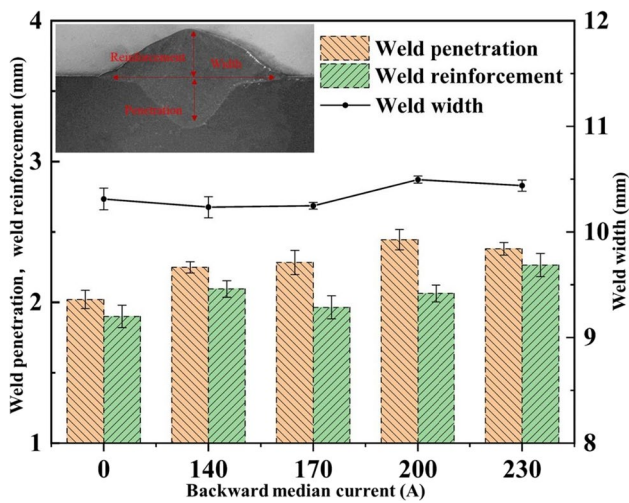


Fig. 6 Macroscopic dimensions of the weld section

force and increasing the weld penetration greater. Welding voltage is the main factor affecting the welding width. In the experiment, the welding voltage remained unchanged, and the welding width remained at about 10.5 mm; the weld reinforcement was slightly less than the weld penetration.

3.2.2 Weld microstructure

Figure 7 shows the microstructure of the weld center prepared by different backward median current waveforms. The

LDU-PMIG weldment microstructure was composed of a large number of irregular and no obvious direction of the lath δ -ferrite, γ -austenite, and a small number of skeletal δ -ferrite, and the uniformity of the microstructure was poor. The microstructure characteristics of weldments prepared by 140 A displayed a large number of skeletal δ -ferrites which were mixed with a certain number of lath δ -ferrites, and the boundaries between different δ -ferrites were not obvious. The weldment microstructure prepared by 230 A backward median current waveform showed a directional skeletal δ -ferrite, and the uniformity of the microstructure was poor. The microstructure of the weldment prepared by the backward median value of 170 A and 200 A showed obvious directivity, the boundary between the microstructure was clear, and the uniformity of the microstructure was good.

The initial solidification phase of the welded weld should be δ -ferrite, but after solidification, part of the δ -ferrite is transformed into γ -austenite, so that the final structure is γ -austenite as matrix, in which the residual δ -ferrite structure, the experimental results agree with the theory [21, 22]. The main factor affecting the microstructure of the remaining ferrite is the cooling rate of the weld. Compared with the land welding, due to the cooling effect of water, many lath and skeletal δ -ferrites were retained in weldment prepared by underwater welding [23]. The instability of the welding process leads to an extremely uneven distribution of the heat source, which greatly affects the microstructure of the weldments. The reason for the good microstructure uniformity

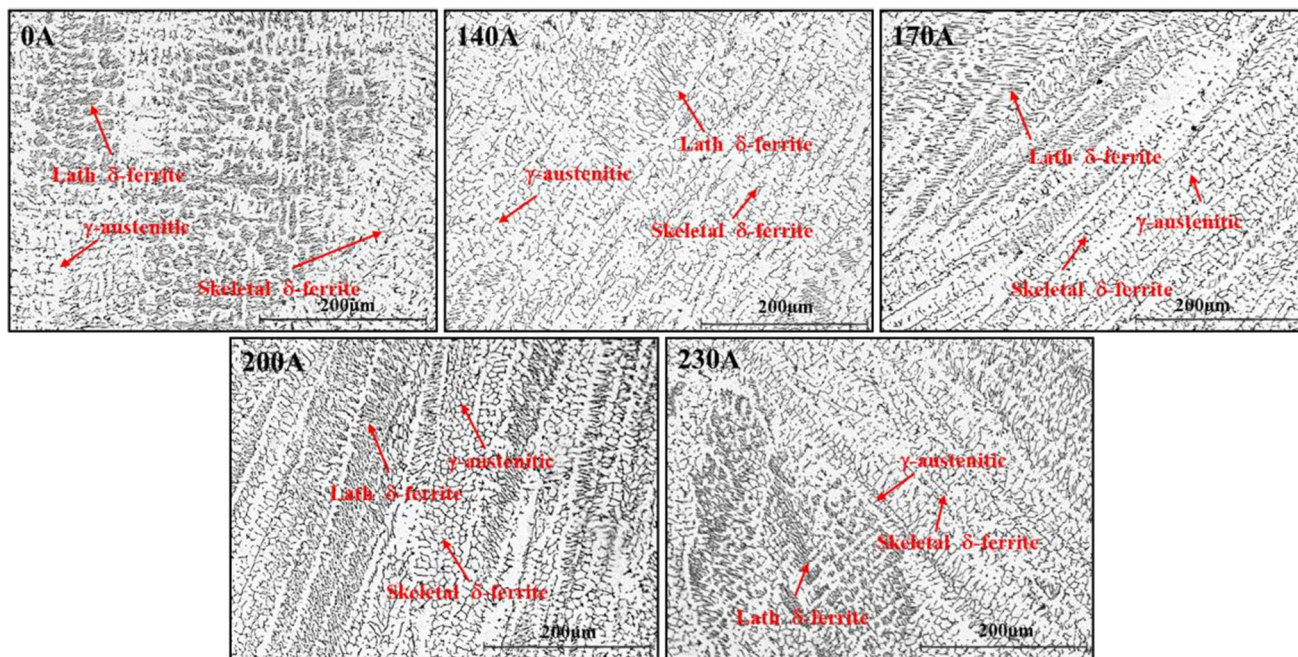


Fig. 7 Weld microstructure

and directivity of the weldments produced by the median value of 170 A and 200 A is that the heat input is stable in the stable welding process, which is conducive to the uniform growth of metal crystals. According to the crystal growth theory, the crystal growth direction is always along the direction of the maximum temperature gradient in the welding pool, so when the heat input of welding is stable, the weld microstructure shows good directivity [24, 25].

3.3 Mechanical properties

Figure 8a displays the stress–strain curves of the weldment prepared by different backward median currents. The stress–strain curves of different weldments in the figure showed a similar growth trend as that of the base material; each curve shows no significant yield stage. The fracture mode was ductile fracture, and the fracture position of each sample was in the weld area, indicating that the tensile

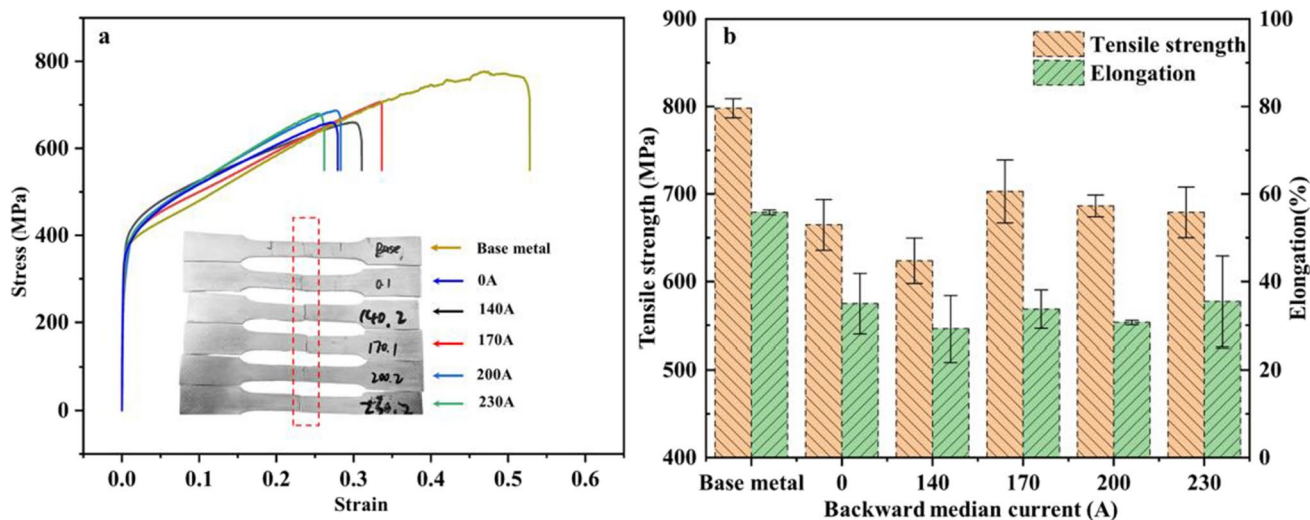


Fig. 8 Test results of mechanical properties: a tensile curve, b tensile strength and elongation

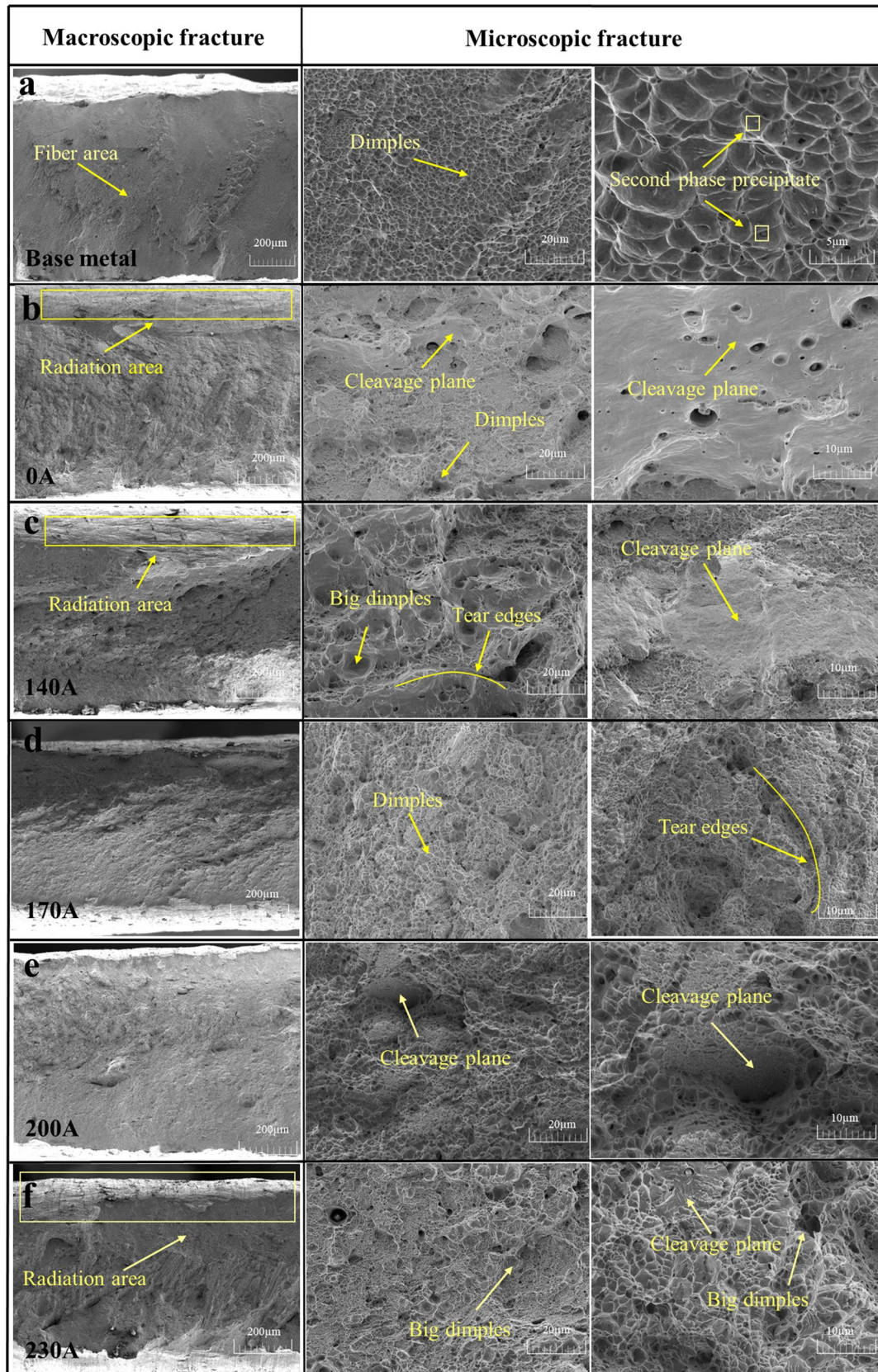


Fig. 9 Fracture morphology of base metal and weldments

strength of the weldment decreased compared with the base material.

Figure 8b shows the average tensile strength and elongation for LDU-PMIG and LDU-BMPMIG weldments. With the increase of backward median current, the average tensile strength of weldments presented a trend of first increasing and then decreasing. The average tensile strength of base metal was 799 MPa and the elongation reached 55.7%. The weldment prepared by backward median current of 170 A exhibited the maximum mean tensile strength of 703 MPa, reaching 87.9% of base metal, but the average tensile strength of weld demonstrated great fluctuation. The average tensile strength of the weldment prepared by 200 A backward current reached 686 MPa, which reached 97.58% of the weldment prepared by 170 A, whereas the standard deviation of weld tensile strength was the smallest. The elongation of the weldments under different median parameters was about 30%, which was half of base metal. With the increase of backward median current, the elongation changed was small and did not show a noticeable change rule; the standard deviation of weld elongation decreased first and then increased. The standard deviation of weld elongation was minimum when the backward median current was 200 A. The weldment prepared by 200 A backward median current showed better mechanical properties and the best mechanical properties stability.

The fracture morphologies of PMIG and BMPMIG weldments are shown in Fig. 9. The base metal sample exhibited higher tensile strength and elongation than the weld sample. Macroscopically, the base metal fracture manifested obvious necking phenomenon, and the fracture was a flat fibrous area. Microscopically, the base metal fracture was composed of a large number of equiaxial dimples, in which the second phase precipitated particles can be seen, and the fracture belongs to ductile fracture. The fracture morphologies of weldments prepared with different backward current waveforms show different characteristics from base metal fracture. In the PMIG weldment fracture, the macroscopic appearance was radiative area, and the microscopic appearance showed large dimples and holes; the dimples were of uneven size, and there were large areas of smooth cleavage surfaces. The macroscopic appearance of the weldment prepared by the backward median current waveform of 170 A and 200 A was fibrous zone; the microscopic morphology consisted of a large number of equiaxial dimples, and no large cleavage plane areas were present. A larger radiation zone appeared in the macroscopic morphology of the weldment produced by 140 A and 230 A; the smooth cleavage surface, large size dimples, and holes appeared in the microstructure of the weldment fracture.

The fracture characteristics of the weldments prepared by different backward median current waveforms remain consistent with the results of the mechanical properties tests; the

fracture type of the weldments changes from ductile fracture of the base material to quasi-dissociative fracture. From the mechanical test results, the stable welding process effectively improved the mechanical properties of the weldment, with the increase of backward median current; weld tensile strength changed in the same trend as the welding stability; the mechanical properties of the weld prepared in the stable welding process showed least fluctuation. The weldment microstructure uniformity was better in the stable welding process; the grain size difference was minor. When the grain was subjected to external force, the external force was uniformly distributed to each grain; the stress concentration was small to obtain a better tensile strength [26].

4 Conclusions

Local dry underwater backward median pulse MIG welding (LDU-BMPMIG) was proposed in this study. The experiment was conducted based on SUS304 stainless steel plate with a thickness of 5 mm, and the influence of the backward median current on the welding stability of LDU-BMPMIG and the mechanical properties of the weld was studied. The outstanding conclusions are as follows:

1. The backward median current waveform remarkably enhanced the welding process stability. With the increase of backward median current, the welding stability firstly increased and then decreased; the most stable welding process appeared at the backward median current of 200 A.
2. The weldment was formed admirably without obvious defects under the appropriate backward median value. With the increase of the backward median value, the weld penetration first increased and then decreased.
3. The microstructure of the LDU-BMPMIG weld was composed of γ -austenite, skeletal δ -ferrite, and lath δ -ferrite. The stable welding process resulted in the microstructure of the weld with satisfied uniformity.
4. The weld fracture type was quasi-cleavage fracture, and the LDU-BMPMIG weldments showed greater average tensile strength. With the increase of the backward median current, the tensile strength increased first and then decreased. The weldment prepared by 200 A showed considerable mechanical properties with minimal fluctuation, which reached 97.58% of maximum average tensile strength.

Acknowledgements The authors are thankful to editors and reviewers.

Author contribution The conceptualization and manuscript were conducted by Wenxu Zhang. The experiments were designed by Haipeng

Liao and Bin Zhang; funding acquisition and manuscript review were performed by Qin Zhang, Xiangmiao Wu, Jiyu Tian, and Zhenmin Wang. All the authors took part in the paper.

Funding This work was supported by the National Natural Science Foundation of China (grant number U2141216); Key Technical Projects of Shenzhen City (grant number JSGG20201201100401005, grant number JSGG20201201100400001); Marine Economic Development (Six Marine Industries) Special Funding Project of Guangdong Province (grant number GDNRC[2021]46); and Science and Technology Planning Project of Guangdong Province (grant number 2021B1515420006; grant number 2021B1515120026).

Data availability The datasets generated and/or analyzed during the current study are available from the corresponding authors on reasonable request.

Declarations

Ethics approval Not applicable.

Consent to participate Not applicable.

Consent for publication Written informed consent for publication was obtained from all participants.

Conflict of interest The authors declare no competing interests.

References

- Gao H, Jiao X, Zhou C, Shen Q, Yu Y (2011) Study on remote control underwater welding technology applied in nuclear power station. *Proc Eng* 15:4988–4993. <https://doi.org/10.1016/j.proeng.2011.08.927>
- Vashishtha P, Wattal R, Pandey S, Bhadauria N (2022) Problems encountered in underwater welding and remedies- a review. *Mater Today Proc* 64:1433–1439. <https://doi.org/10.1016/j.matpr.2022.04.634>
- Surojo E, Syah Putri EDW, Budiana EP, Triyono, (2020) Recent developments on underwater welding of metallic material. *Proc Struct Integr* 27:14–21. <https://doi.org/10.1016/j.prostr.2020.07.003>
- Han LG, Wu XM, Chen GD, Wang ZM, Fan WY (2019) Local dry underwater welding of 304 stainless steel based on a microdrain cover. *J Mater Process Tech* 268:47–53. <https://doi.org/10.1016/j.jmatprotec.2018.12.029>
- Wang ZM, Pei K, Han LG, Wu HD, Lin SB, Cai XY, Xu MJ, Zhang Q (2021) Effect of pulse frequency on droplet transfer and weld formation in local dry underwater welding. *J Manuf Process* 68:1726–1734. <https://doi.org/10.1016/j.jmapro.2021.06.065>
- Liao HP, Zhang WX, Li XY, Pei K, Lin SB, Tian JY, Wang ZM (2022) Numerical simulation and experimental verification of droplet transfer during local dry underwater MIG welding process of SUS304. *J Mater Res Technol* 21:1960–1973. <https://doi.org/10.1016/j.jmrt.2022.10.040>
- Liao HP, Zhang WX, Li XY, Pei K, Lin SB, Tian JY, Wang ZM (2022) Effect of pulse current on droplet transfer behavior and weld formation of 304 stainless steel in local dry underwater pulse MIG welding. *Int J Adv Manuf Tech* 122(2):869–879. <https://doi.org/10.1007/s00170-022-09938-y>
- Guo N, Cheng Q, Fu YL, Du YP, Zhang X, Feng JC (2019) Investigation on the mass transfer control, process stability and welding quality during underwater pulse current FCAW for Q235. *J Manuf Process* 46:317–327. <https://doi.org/10.1016/j.jmapro.2019.08.022>
- Reza Tabrizi T, Sabzi M, Mousavi Anijdan SH, Eivani AR, Park N, Jafarian HR (2021) Comparing the effect of continuous and pulsed current in the GTAW process of AISI 316L stainless steel welded joint: microstructural evolution, phase equilibrium, mechanical properties and fracture mode. *J Mater Res Technol* 15:199–212. <https://doi.org/10.1016/j.jmrt.2021.07.154>
- Wu KY, Zhan JT, Cao XW, Zeng M, Ding N (2020) Metal transfer of aluminum alloy double-wire pulsed GMAW with a median waveform. *J Mater Process Tech* 286:116761. <https://doi.org/10.1016/j.jmatprotec.2020.116761>
- Xu J, Ma Y, Wang L, Zhang Y, Lu X (2022) Numerical investigation on the influence of current waveform on droplet transfer in pulsed gas metal arc welding. *Vacuum* 203:111230. <https://doi.org/10.1016/j.vacuum.2022.111230>
- Wu J, Wang Z, Lin S, Xie Z, Xu M, Tian J, Guo C (2022) Effect of fast-frequency pulsed waveforms on the microstructure and mechanical properties of Ti–6Al–4V alloy welded by FFP-TIG. *J Mater Res Technol* 20:516–531. <https://doi.org/10.1016/j.jmrt.2022.07.126>
- Huang Y, Yang DQ, Wang KH, Wang L, Zhou Q (2020) Stability analysis of GMAW based on multi-scale entropy and genetic optimized support vector machine. *Measurement* 151:107282. <https://doi.org/10.1016/j.measurement.2019.107282>
- Yao P, Zhou K, Zhu Q (2017) Quantitative evaluation method of arc sound spectrum based on sample entropy. *Mech Syst Signal Pr* 92:379–390. <https://doi.org/10.1016/j.ymsp.2017.01.016>
- Nie J, Ma JR, Shi Y (2015) Correlation between stability of aluminium alloy pulsed metal-inert gas welding and pulse current signal. *Mater Res Innov* 19:674–678. <https://doi.org/10.1179/1432891714Z.0000000001174>
- Liao HP, Zhang WX, Xie HM, Li XY, Zhang Q, Wu XM, Tian JY, Wang ZM (2023) Effects of welding speed on welding process stability, microstructure and mechanical performance of SUS304 welded by local dry underwater pulsed MIG. *J Manuf Process* 88:84–96. <https://doi.org/10.1016/j.jmapro.2023.01.047>
- Planckaert JP, Djerroune E, Brie D, Briand F, Richard F (2010) Modeling of MIG/MAG welding with experimental validation using an active contour algorithm applied on high speed movies. *Appl Math Model* 34(4):1004–1020. <https://doi.org/10.1016/j.apm.2009.07.011>
- Zhao D, Wang Y, Liang D, Ivanov M (2020) Performances of regression model and artificial neural network in monitoring welding quality based on power signal. *J Mater Res Technol* 9(2):1231–1240. <https://doi.org/10.1016/j.jmrt.2019.11.050>
- Pincus SM (1991) Approximate entropy as a measure of system complexity. *P Natl Acad Sci Usa* 88:2297–301
- Chen C, Sun GR, Du WB, Li Y, Fan CL, Zhang HJ (2022) Influence of heat input on the appearance, microstructure and microhardness of pulsed gas metal arc welded Al alloy weldment. *J Mater Res Technol* 21:121–130. <https://doi.org/10.1016/j.jmrt.2022.09.028>
- Guo N, Fu YL, Xing X, Liu YK, Zhao SX, Feng JC (2018) Underwater local dry cavity laser welding of 304 stainless steel. *J Mater Res Technol* 260:146–155. <https://doi.org/10.1016/j.jmatprotec.2018.05.025>
- Fu JW, Yang YS, Guo JJ, Ma JC, Tong WH (2008) Formation of a two-phase microstructure in Fe–Cr–Ni alloy during directional solidification. *J Cryst Growth* 311(1):132–136. <https://doi.org/10.1016/j.jcrysgro.2008.10.021>
- Di XJ, Ji SX, Cheng FJ, Wang DP, Cao J (2015) Effect of cooling rate on microstructure, inclusions and mechanical properties

- of weld metal in simulated local dry underwater welding. *Mater Design* 88:505–513. <https://doi.org/10.1016/j.matdes.2015.09.025>
24. Vashishtha H, Taiwade RV, Sharma S (2017) Effect of electrodes and post weld solution annealing treatment on microstructures, mechanical properties and corrosion resistance of dissimilar high nitrogen austenitic and conventional austenitic stainless steel weldments. *Mater Trans* 58(2):182–185. <https://doi.org/10.2320/matertrans.M2016175>
25. Ramkumar KD, Abraham WS, Viyash V, Arivazhagan N, Rabel AM (2017) Investigations on the microstructure, tensile strength and high temperature corrosion behaviour of Inconel 625 and Inconel 718 dissimilar joints. *J Manuf Process* 25:306–322. <https://doi.org/10.1016/j.jmapro.2016.12.018>
26. Fan YH, Zhang B, Wang JQ, Han EH, Ke W (2019) Effect of grain refinement on the hydrogen embrittlement of 304 austenitic stainless steel. *J Mater Sci Technol* 35(10):2213–2219. <https://doi.org/10.1016/j.jmst.2019.03.043>

Publisher's note Springer Nature remains neutral with regard to jurisdictional claims in published maps and institutional affiliations.

Springer Nature or its licensor (e.g. a society or other partner) holds exclusive rights to this article under a publishing agreement with the author(s) or other rightsholder(s); author self-archiving of the accepted manuscript version of this article is solely governed by the terms of such publishing agreement and applicable law.